JCI The Journal of Clinical Investigation

mTORC1-to-AMPK switching underlies β cell metabolic plasticity during maturation and diabetes

Rami Jaafar, … , Suneil K. Koliwad, Anil Bhushan

J Clin Invest. 2019;129(10):4124-4137. https://doi.org/10.1172/JCI127021.

Research Article **Endocrinology**

Pancreatic β cells differentiate during fetal life, but only postnatally acquire the capacity for glucose-stimulated insulin secretion (GSIS). How this happens is not clear. In exploring what molecular mechanisms drive the maturation of β cell function, we found that the control of cellular signaling in β cells fundamentally switched from the nutrient sensor target of rapamycin (mTORC1) to the energy sensor 5′-adenosine monophosphate–activated protein kinase (AMPK), and that this was critical for functional maturation. Moreover, AMPK was activated by the dietary transition taking place during weaning, and this in turn inhibited mTORC1 activity to drive the adult β cell phenotype. While forcing constitutive mTORC1 signaling in adult β cells relegated them to a functionally immature phenotype with characteristic transcriptional and metabolic profiles, engineering the switch from mTORC1 to AMPK signaling was sufficient to promote β cell mitochondrial biogenesis, a shift to oxidative metabolism, and functional maturation. We also found that type 2 diabetes, a condition marked by both mitochondrial degeneration and dysregulated GSIS, was associated with a remarkable reversion of the normal AMPK-dependent adult β cell signature to a more neonatal one characterized by mTORC1 activation. Manipulating the way in which cellular nutrient signaling pathways regulate β cell metabolism may thus offer new targets to improve β cell function in diabetes.

mTORC1-to-AMPK switching underlies β cell metabolic plasticity during maturation and diabetes

Rami Jaafar,[1] Stella Tran,[1] Ajit N. Shah,[1] Gao Sun,[2] Martin Valdearcos,[1] Piero Marchetti,[3] Matilde Masini,[3] Avital Swisa,[4] Simone Giacometti,[1] Ernesto Bernal-Mizrachi,[5] Aleksey Matveyenko,[6] Matthias Hebrok,[1] Yuval Dor,[4] Guy A. Rutter,[2] Suneil K. Koliwad,[1] and Anil Bhushan[1]

[1]The Diabetes Center, UCSF, San Francisco, California, USA. [2]Section of Cell Biology and Functional Genomics, Department of Medicine, Imperial College London, Hammersmith Hospital London, United Kingdom. [3]Department of Clinical and Experimental Medicine, University of Pisa, Pisa, Italy. [4]Department of Developmental Biology and Cancer Research, Institute for Medical Research Israel-Canada, Hebrew University-Hadassah Medical School, Jerusalem, Israel. [5]Division of Endocrinology, Diabetes and Metabolism, University of Miami, Miller School of Medicine, Miami, Florida, USA. [6]Department of Physiology and Biomedical Engineering, Mayo Clinic, Rochester, Minnesota, USA.

Pancreatic β cells differentiate during fetal life, but only postnatally acquire the capacity for glucose-stimulated insulin secretion (GSIS). How this happens is not clear. In exploring what molecular mechanisms drive the maturation of β cell function, we found that the control of cellular signaling in β cells fundamentally switched from the nutrient sensor target of rapamycin (mTORC1) to the energy sensor 5′-adenosine monophosphate–activated protein kinase (AMPK), and that this was critical for functional maturation. Moreover, AMPK was activated by the dietary transition taking place during weaning, and this in turn inhibited mTORC1 activity to drive the adult β cell phenotype. While forcing constitutive mTORC1 signaling in adult β cells relegated them to a functionally immature phenotype with characteristic transcriptional and metabolic profiles, engineering the switch from mTORC1 to AMPK signaling was sufficient to promote β cell mitochondrial biogenesis, a shift to oxidative metabolism, and functional maturation. We also found that type 2 diabetes, a condition marked by both mitochondrial degeneration and dysregulated GSIS, was associated with a remarkable reversion of the normal AMPK-dependent adult β cell signature to a more neonatal one characterized by mTORC1 activation. Manipulating the way in which cellular nutrient signaling pathways regulate β cell metabolism may thus offer new targets to improve β cell function in diabetes.

Introduction

During the neonatal period, pancreatic islets progressively lose their proliferative capacity and develop instead the capacity for highly sensitive and robust glucose-stimulated insulin secretion (GSIS) (1). This functional maturation is complex, involving both metabolic and transcriptional remodeling of pancreatic β cells (2, 3). However, the specific cues and responsive molecular mechanisms mediating this cellular remodeling remain poorly understood.

Previous studies suggest that β cell maturation and the capacity for GSIS are regulated by a diverse set of factors. First, altered macronutrient consumption initiated upon weaning is associated with changes in islet microRNA (miR) levels (4, 5). Next, the transition induced during weaning is associated with enhanced glucose-stimulated oxidative phosphorylation and insulin secretion (6), the induction of key β cell–specific transcription factors promoting mitochondrial function and oxidative metabolism (3, 7, 8), and expression of UCN3, an essential marker of mature β cells (1). Weaning is also associated with methylation-dependent repression of transcripts involved in anaerobic glycolytic metabolism (2). Together, these changes support the notion that the induction of GSIS, and the corresponding attenuation of proliferation, among β cells are associated with a remodeling of cellular metabolism. However, the signaling hierarchy, in particular master regulators, in charge of this remodeling remains elusive.

The mammalian target of rapamycin (mTOR) is a nutrient-sensitive kinase critical for the regulation of postnatal pancreatic β cell proliferation and growth (9, 10). Two mTOR complexes exist, mTORC1 and mTORC2, reflecting differences in regulation and subunit composition (11). Several reports show that mTORC1 promotes β cell proliferation in utero and during the neonatal period (12, 13) through the regulation of cyclins D2 and D3, and CDK4 (9). Furthermore, β cell–specific ablation of TSC1 or TSC2 (the upstream inhibitors of mTOR) results in increased postnatal β cell mass (10, 14, 15). On the other hand, β cell–specific deletion of mTORC1 in mice results in severe glucose intolerance due to underdeveloped β cell mass (16–18). Collectively, these data indicate that mTORC1 expression is required for the development and growth of β cells during embryonic and early postnatal life.

Authorship note: SKK and AB contributed equally to this work.
Conflict of interest: GS reports current employment income from Pegbio (Suzhou) Co., Ltd. MH reports equity in Semma, Encellin, and Viacyte, income from Semma, and research support from Eli Lilly & Co. GR reports research support from Servier and income from Sun Pharmaceuticals. SK reports income from, and equity in, Suggestic, consulting income from Astra Zeneca and Bristol Myers Squibb, and research support from Gilead Sciences and Calico Labs. AB reports income from, and equity in, Deciduous Therapeutics, and a US Patent (PCT/US18/31161) held by UCSF.

Submitted: December 21, 2018; **Accepted:** June 24, 2019; **Published:** August 26, 2019.
Reference information: *J Clin Invest*. 2019;129(10):4124–4137.
https://doi.org/10.1172/JCI127021.

5′-Adenosine monophosphate–activated protein kinase (AMPK) is a master sensor of cellular energy status (19) and a potent inhibitor of mTORC1 activity (20, 21). Its kinase activity is regulated by the intracellular ratio of ATP versus AMP/ADP, serving as a key sensor for energy stress (22). In opposition to mTORC1, AMPK has an evolutionarily conserved role in restraining cellular growth and proliferation in response to limitations in cellular energy availability (22). Moreover, deleting LKB1 (an upstream AMPK activator) increases β cell proliferation and mass by inducing the mTORC1 pathway, resulting in enhanced insulin output (23–25). Furthermore, work from our group and others using mice lacking both AMPKα1 and -α2 highlights the importance of AMPK for a mature β cell phenotype, including adult-like insulin secretory characteristics (25–27).

Here we show, using both genetic and nutritional approaches, that a concerted switch from mTORC1- to AMPK-dependent cellular signaling mediates the manifestation of several features that define functional β cell maturation. Furthermore, we show that this same switch, when engaged in the reverse direction, underlies a process leading to β cell dysfunction in driving type 2 diabetes (T2D). In sum, the reciprocal opposition between mTORC1 and AMPK determines whether β cells adopt a more proliferative, immature phenotype, or the mature, highly insulin-responsive phenotype essential for postnatal life.

Results

β Cells switch from mTORC1- to AMPK-dependent signaling during postnatal maturation. To identify pathways critical for β cell maturation, we performed RNA sequencing (RNAseq) on neonatal and adult β cells from mouse pancreata. Islets from MIP-GFP mice were harvested on postnatal days 6 and 45, dispersed, and β cells were isolated by fluorescence-activated cell sorting (FACS) (Figure 1A). Principal component analysis (PCA) of these RNAseq data showed that the neonatal (P6) β cell replicates cluster together, away from the adult (P45) replicates (Supplemental Figure 1, A and B; supplemental material available online with this article; https://doi.org/10.1172/JCI127021DS1). Gene set enrichment analysis (GSEA) (28) showed that the neonatal β cell transcriptome is enriched for pathways regulating the cell cycle, whereas adult β cell transcriptomes are enriched for genes comprising the citrate (TCA) cycle and mitochondrial electron transport chain (Supplemental Figure 1C).

Analysis of specific genes related to either β cell proliferation (*Nek2*, *Cenpf*, *Cenpe*, *Mki67*, *Cdk1*, *Rfc5*, *Ccna2*, and *Pole*) or β cell maturation (*Ins1*, *Ins2*, *Ucn3*, *G6pc2*, *Ero1lb*, *Syt4*, *Pcsk1*, and *Mafb*) confirmed that immature neonatal β cells have higher mRNA levels of proliferation markers, and that by adulthood this phenotype switches to one characterized by the induction of mRNA encoding indicators of maturation (Supplemental Figure 1D). This clearly evident switch confirmed the quality and reliability of our RNAseq data sets.

Further analysis of the RNAseq data revealed that the levels of mRNA encoding AMPK and mTORC1 pathway–regulated transcripts were markedly different between neonatal and adult β cells. Specifically, the expression of mTORC1 activator and effector genes was elevated in neonatal β cells, whereas genes in the AMPK pathway (*Prkaa2* and *Pten*) were induced in adult β cells (Figure 1B).

We next assessed the activation of mTORC1 in pancreatic islets by immunofluorescence using the Ser240/244 phosphorylation of its downstream target rpS6 as readout. We found that mTORC1 is highly active in neonatal β cells, but that this activation is dramatically decreased around P18 and is undetectable in adult β cells (Figure 1C). FACS analysis confirmed this observation, showing that cells doubly positive for insulin and phospho-rpS6 (p-rpS6) comprised 20% of the cells in neonatal islets, but only 5% of the cells in adult islets (Figure 1D).

Of note, we also observed heterogeneous mTORC1 activity in cell types surrounding the islets of both neonatal and adult mice. Indeed, mTORC1 is a common controller of cellular energy metabolism, and its activation in exocrine cell types has been shown (18, 29), suggesting this observation was to be expected.

To further dissect the process of β cell maturation and the mechanism underlying mTORC1 inhibition in adult islets, we assessed the expression and activity of AMPK, an upstream regulator and inhibitor of mTORC1 (20, 21) in both neonatal and adult islets. In line with the RNAseq data, immunoblotting showed that total AMPK catalytic α subunit protein abundance is substantially lower in neonatal islets than adult islets (Figure 1E). Additionally, although AMPK activity (α subunit p-Thr172) in cultured islets was generally reduced by increasing extracellular glucose concentration (2.8 mM to 16.7 mM) as described previously (30, 31), both total and p-AMPK were consistently elevated in the β cells of adult versus neonatal islets (Figure 1E). These data indicate that β cells, which represent 60%–80% of mouse pancreatic islets (32), undergo a pronounced induction of both AMPK expression and activity during the neonatal-to-adult transition.

Moreover, the pattern of AMPK activity in the context of isolated islets was reciprocal to that of mTORC1. For example, whereas total and p-AMPK were increased in adult versus neonatal islets, the opposite was true for p-rpS6 (Figure 1E). Moreover, whereas p-AMPK was relatively reduced by switching adult islets from low to high glucose, mTORC1 activity measured concomitantly was relatively increased by this switch (Figure 1E and Supplemental Figure 1E).

We also measured levels of p-AMPK (Thr172) in pancreatic sections, a convenient proxy for in situ AMPK activation, though we note that AMPK is also regulated by AMP, ADP, and direct allosteric mechanisms (19). Whereas no neonatal β cells stained for p-AMPK ($n = 30$ islets, 4 mice per group), adult β cells were robustly positive for p-AMPK by comparison (Figure 1F). All of these data together highlight the intriguing concept that the transition of pancreatic β cells from neonatal to adult life occurs in the context of a fundamental switch from mTORC1 to AMPK-dependent signaling.

Weaning from maternal milk induces the switch from mTORC1 to AMPK signaling in β cells. To investigate what regulates the reciprocal relationship between mTORC1 and AMPK signaling in maturing β cells, we analyzed both adult human and adult mouse islets that were treated for 12 hours with either everolimus (an mTORC1 inhibitor) or 5-aminoimiazole-4-carboxamide-1-β-D-ribofuranoside (AICAR, an AMPK activator) (19). As expected, everolimus treatment inhibited mTORC1 activity in β cells, as revealed by a dramatic reduction in specific rpS6 phosphorylation, but hardly altered AMPK phosphorylation. By contrast, AICAR treatment was sufficient to both activate AMPK and completely abrogate mTORC1 phosphorylation in both mouse and human islets (Figure 2, A and B, with associated quantifications in Supplemental Figure 2, A and B). Taken together, these findings indicate that

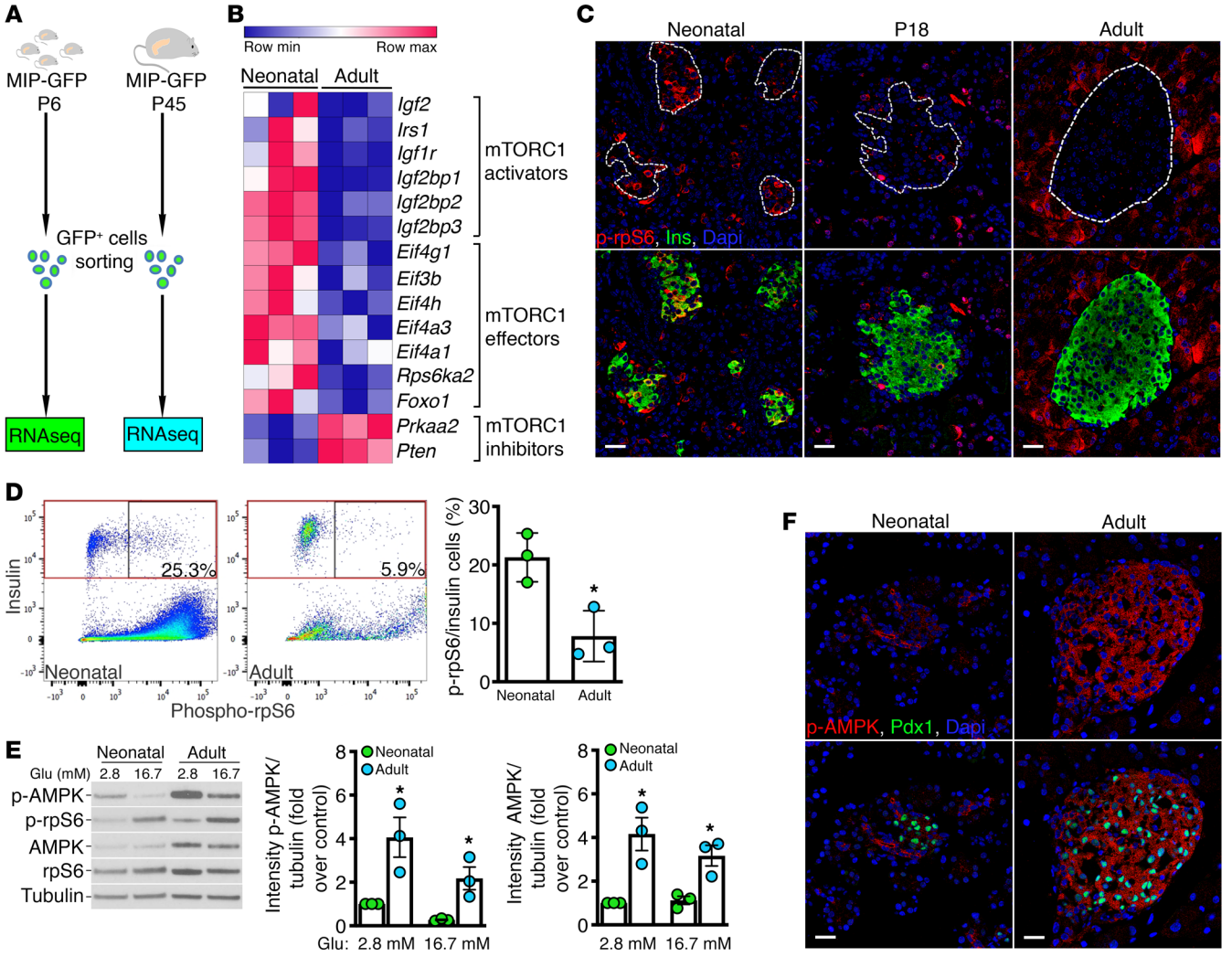

Figure 1. β Cells switch from mTORC1 to AMPK-dependent signaling during postnatal maturation. (**A**) Experimental paradigm for RNAseq on sorted pancreatic β cells in mice at P6 and P45. (**B**) Heatmap, showing the expression profile of genes related to mTORC1/AMPK signaling in β cells at P6 and P45. In this comparison, deepening colors represent progressively lower (blue) or higher (red) mRNA levels for any given gene ($P < 0.05$). (**C**) Representative pancreatic sections from WT mice at P6, P18, and 2 months of age stained for insulin (green) and p-rpS6 (red). Nuclei were counterstained with DAPI (blue). Scale bars: 50 μm. (**D**) Quantification (FACS) of the number of cells positive for both insulin and p-rpS6 in P7 and 2-month-old WT mice. Data shown are representative of 3 separate experiments. *$P = 0.0178$ (2-tailed unpaired *t* test). (**E**) Immunoblot representing an experiment repeated 3 times ($n = 3$ for each), showing total rpS6, p-rpS6 (Ser240/244), p-AMPK (Thr172), and total AMPK in neonatal and adult islets treated with either 2.8 mM or 16.7 mM glucose. β-Tubulin was used as loading control. Corresponding p-AMPK and total AMPK normalized to β-tubulin quantifications are adjacent. Five to 7 P6 mice and 1 adult mouse were used for each replicate. *$P < 0.01$ (unpaired *t* test corrected for multiple comparison using the Holm-Sidak method). (**F**) Representative pancreatic sections from WT mice at P6 and 2 months of age stained for Pdx1 (green) and p-AMPK (red), with DAPI (blue) counterstaining the nuclei. Scale bars: 50 μm.

inhibiting mTORC1 activity is not sufficient on its own to activate AMPK in β cells, but that activating AMPK is sufficient to repress mTORC1. This unidirectional relationship supports the concept that AMPK, as in other systems, is a key repressor of mTORC1 in β cells. Indeed, its activation is responsible for shutting off mTORC1 signaling, triggering a key step in β cell maturation.

The process of weaning, which in mice starts in the third week of life, is associated with decreased reliance on the consumption of fat-rich maternal milk in favor of an adult-type diet with a more carbohydrate-rich macronutrient composition (33). Given the role of mTORC1 as a nutrient-sensing kinase, we hypothesized that postnatal β cell maturation may represent an adaptation to the cessation of milk consumption, and that mTORC1 repression through AMPK activation may act as a physiological mediator of this process.

To test this hypothesis, we enabled mice to continue to consume a diet highly enriched for milk fat by giving them access to a milk fat–rich diet and supplementing this with daily milk fat gavage, beginning at P11–P13 and continuing through adulthood (P40). This allowed us to maintain high milk fat consumption in the mice during the period over which weaning normally occurs. Remarkably, allowing mice to continue assimilating milk fat throughout their entry into adulthood, a period during which this is usually declining, was sufficient to allow β cells to maintain neo-

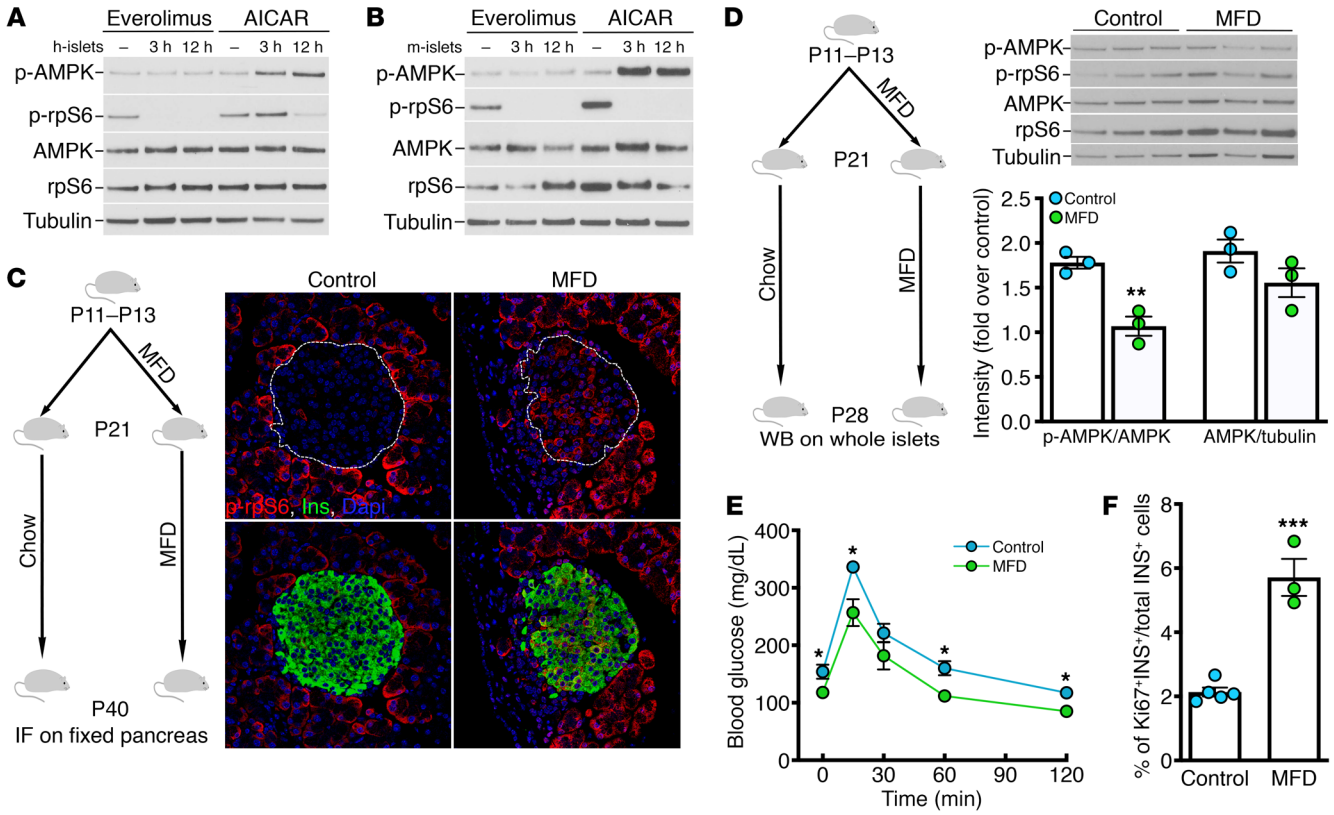

Figure 2. Weaning from maternal milk induces the switch from mTORC1 to AMPK signaling in β cells. (**A** and **B**) Representative immunoblots showing p-AMPK, p-rpS6, total AMPK, total rpS6, and β-tubulin in (**A**) adult human islets and (**B**) adult mouse islets after treatment with 1 mM AICAR or 40 μM everolimus for the indicated time (n = 3 for both human and mouse islets except only for the 3-hour AICAR treatment condition, where n = 2). (**C**) Experimental paradigm for the milk fat–supplemented diet (MFD), and immunofluorescence (IF) staining for insulin (green) and p-rpS6 (red) in representative pancreatic sections from P40 mice otherwise fed either standard chow (control) or the MFD. Nuclei were counterstained with DAPI (blue). Original magnification, ×64. (**D**) Experimental paradigm for the MFD and associated representative Western blots (WB), showing p-AMPK, p-rpS6, total S6, and total AMPK in control and MFD mice. β-Tubulin was used as loading control. Quantification of p-AMPK/AMPK and AMPK/β-tubulin is shown below. $^{**}P$ = 0.0062 (unpaired t test corrected for multiple comparisons using the Holm-Sidak method). (**E**) Intraperitoneal glucose tolerance test in control and MFD mice (n = 7). $^{*}P < 0.05$ (unpaired t test corrected for multiple comparisons using the Holm-Sidak method). (**F**) Percentage of Ki67^{+} and insulin^{+} cells in control and MFD islets (n = 3–5). $^{***}P$ = 0.0002 (2-tailed unpaired t test).

natal levels of mTORC1 activity, which was otherwise completely repressed in the control mice (Figure 2C).

We next assessed the expression and phosphorylation of β cell AMPK and rpS6 in the islets of these mice. Unlike the AMPK activation seen in the islets of adult mice weaned onto standard chow, islets from mice that continued milk fat consumption past weaning displayed a marked suppression of AMPK phosphorylation, although not all the way to neonatal levels, despite the entry into adulthood (Figure 2D). Similarly, extending milk fat consumption past weaning tended to produce higher levels of p-rpS6 within the islets of adult mice, though this trend was not significant (Figure 2D and Supplemental Figure 2C).

We also examined whether continuing milk fat consumption from the neonatal period into adulthood in mice impacts β cell function. Mice provided with milk fat by gavage from P11 into adulthood had lower serum glucose levels than did vehicle-treated control mice, both at baseline and during a glucose tolerance test, indicative of constitutively enhanced glucose clearance (Figure 2E and Supplemental Figure 2D). Supporting this, β cell (INS^{+}) area tended to be higher in milk fat-supplemented mice than in controls, though this trend was not statistically significant (Supplemental Figure 2E). Moreover, the percentage of proliferating (Ki67^{+}) β cells was higher in the mice provided milk fat than it was in control mice (Figure 2F). We also found that mRNA levels for the maturity markers *Ins1*, *Ins2*, and *Mafa* were lower in the islets of the mice provided milk fat (Supplemental Figure 2F). Islet mRNA levels of *Ucn3*, by contrast, were not affected, although this is not surprising given that approximately 93% of β cells already express *Ucn3* by P13, which is prior to weaning (1).

These data together highlight that continuing milk fat consumption from the neonatal period into adulthood in mice is sufficient to maintain an immature-cell phenotype, and strongly support the concept that shifting from fat to carbohydrate consumption during weaning is a previously unrecognized mechanistic driver of mTORC1-to-AMPK switching and consequent functional β cell maturation.

mTORC1 maintains the immature phenotype of pancreatic β cells. To definitively test whether mTORC1 is responsible for maintaining the immature phenotype of neonatal pancreatic β cells, we generated Rip-Cre *Tsc1*$^{fl/fl}$ (βTSC1-KO) mice, where TSC1, the

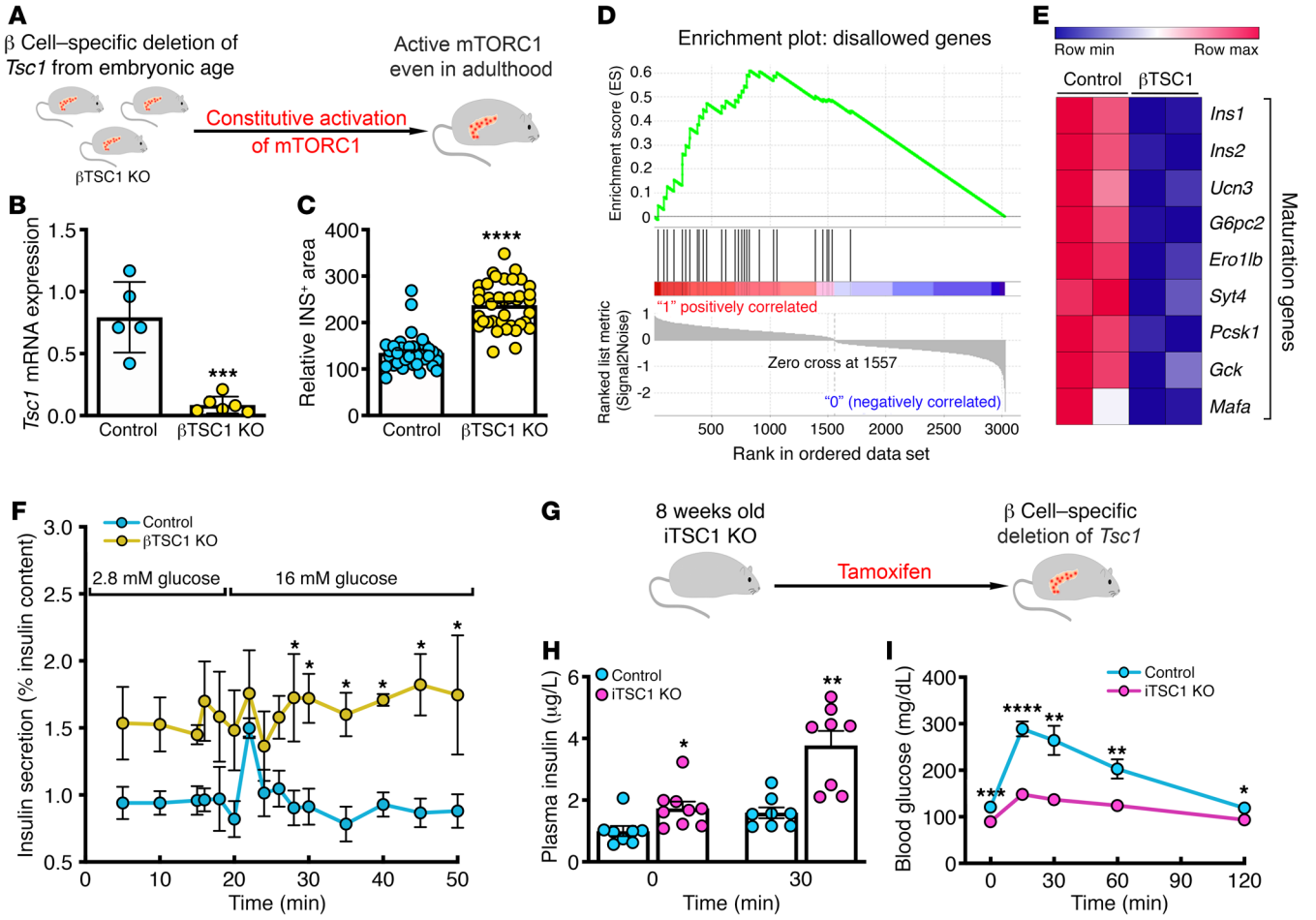

Figure 3. mTORC1 maintains the immature phenotype of pancreatic β cells. (**A**) Genetic model for constitutive activation of mTORC1. (**B**) mRNA levels of *Tsc1* in islets from control and βTSC1-KO mice (n = 7–9). ***P = 0.0002 (2-tailed unpaired t test). (**C**) Relative β cell areas in pancreatic sections from control and βTSC1-KO mice, measured as the ratio of insulin$^+$ area/insulin$^+$ cell number (n = 37–38 islets/group). ****P < 0.0001 (2-tailed unpaired t test). (**D**) GSEA, showing enrichment of disallowed genes in RNAseq data from βTSC1-KO islets (P < 0.05). (**E**) Heatmap, showing the transcriptional profile of β cell maturity markers in βTSC1-KO and control mice (P < 0.05). (**F**) Insulin secretion (percentage of insulin content) in a perifusion assay on βTSC1-KO and control islets exposed to 2.8 mM and 16 mM glucose (n = 4–5). *P < 0.05 (unpaired t test corrected for multiple comparisons using the Holm-Sidak method). (**G**) Model for inducing mTORC1 activation in adult mice. (**H**) Plasma insulin levels after glucose challenge in iTSC1-KO and control mice (n = 8–9). *P = 0.017, **P = 0.0012 (unpaired t test corrected for multiple comparisons using the Holm-Sidak method). (**I**) Intraperitoneal glucose tolerance test in iTSC1-KO and control mice (n = 10–11). *P < 0.05, **P < 0.01, ***P < 0.001, ****P < 0.0001 (unpaired t test corrected for multiple comparisons using the Holm-Sidak method).

upstream negative regulator of mTORC1, is deleted, leading to a constitutive activation of mTORC1 in β cells (Figure 3A). βTSC1-KO mice also carry a YFP allele, having been crossed onto a ROSA26-stop-EYFP line, with the latter serving as a lineage tracing tool to assess Cre expression and genomic recombination. All subsequent experiments were performed using βTSC1-KO mice or littermate (*Tsc1*$^{fl/fl}$; or *Tsc1*$^{+/+}$, Cre$^+$) controls. We confirmed that Cre expression in βTSC1-KO mice is restricted to pancreatic β cells by demonstrating colocalization of insulin and YFP staining (data not shown). Transcriptional analysis confirmed that *Tsc1* mRNA is significantly reduced in islets from βTSC1-KO mice versus those from control mice (Figure 3B). Confirming the direct consequence of deleting TSC1 specifically in β cells, approximately 85% of pancreatic β cells in βTSC1-KO mice had increased specific p-rpS6 staining intensity, indicative of upregulated β cell mTORC1 activity (Supplemental Figure 3, A and B). Measuring pancreatic INS$^+$ area histologically showed that constitutive activation of mTORC1 in adult βTSC1-KO mice increases β cell mass (Figure 3C), mirroring what was seen in response to milk fat gavage.

To more fully determine whether constitutively activating mTORC1 recapitulates an immature islet phenotype in adult mice, we performed RNAseq on islets from adult βTSC1-KO and control mice. We first explored a list of β cell disallowed genes that are known to be upregulated in neonatal islets (2, 34). GSEA showed that adult βTSC1-KO islets were enriched for the expression of such genes (Figure 3D). Moreover, expression of key maturation genes (*Ins1*, *Ins2*, *Unc3*, *G6pc2*, *Erol1b*, *Syt4*, *Pcsk1*, and *Mafa*) was concomitantly reduced in adult βTSC1-KO islets when compared with control islets (Figure 3E). Assessment of MafA by immunostaining mirrored the transcriptional data, as MafA expression was reduced in the islets of βTSC1-KO versus control mice (Supplemental Figure 3C). Together, these data indicate that forcing β cell–specific mTORC1 activation in

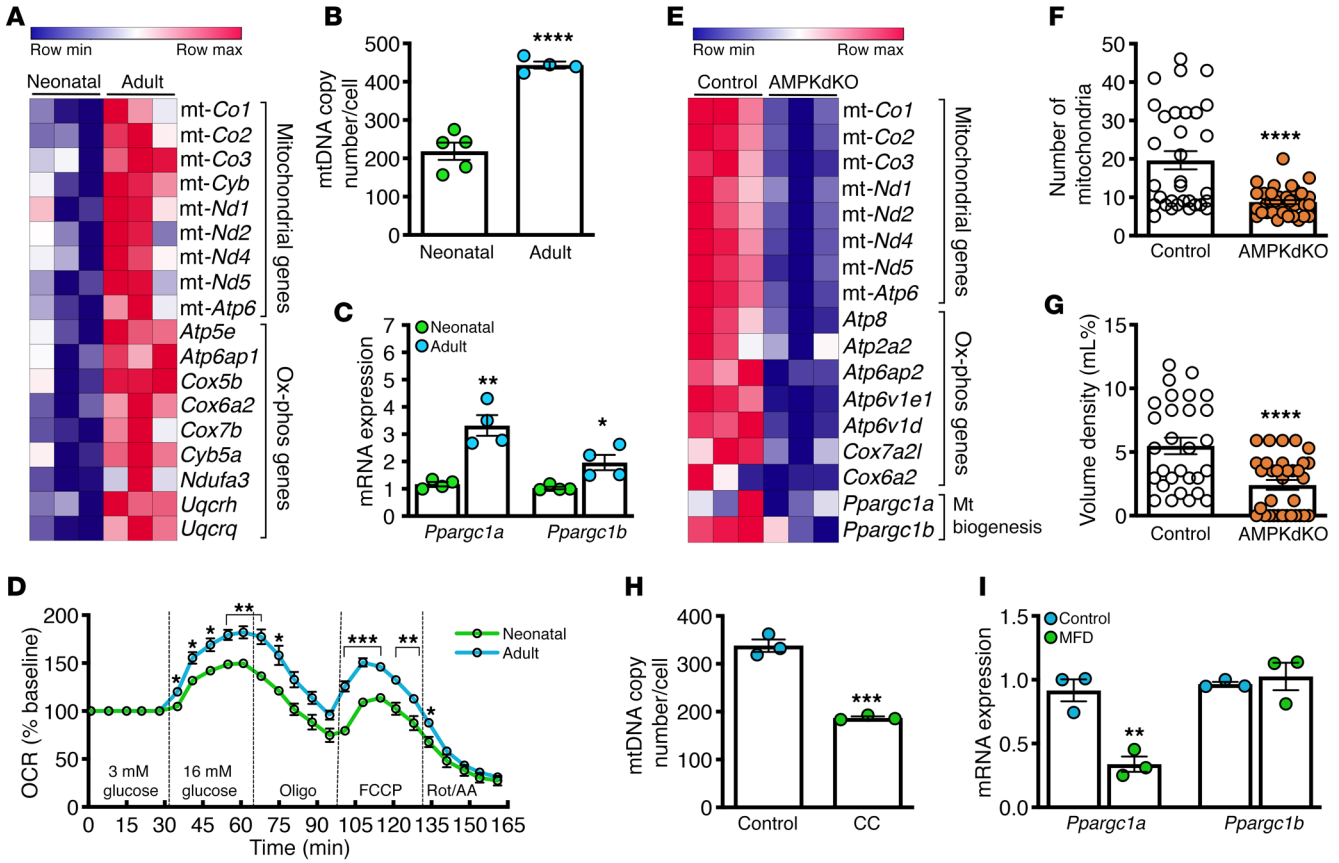

Figure 4. AMPK activation triggers a switch to oxidative metabolism in mature islets. (**A**) Heatmap, profiling mitochondrial genes and genes related to ox-phos metabolism in P6 and P45 β cells ($P < 0.05$). (**B**) qPCR, showing the ratio of mtDNA to nuclear DNA in P6 and adult islets ($n = 4–5$). $^{****}P < 0.0001$ (2-tailed unpaired *t* test). (**C**) Relative *Ppargc1a* and *Ppargc1b* mRNA levels in P6 and adult islets ($n = 4$). $^{*}P = 0.016$, $^{**}P = 0.0029$ (unpaired *t* test corrected for multiple comparisons using the Holm-Sidak method). (**D**) Oxygen consumption rates for cultured neonatal and adult islets (Seahorse XF24), with data presented relative to baseline ($n = 7–8$). $^{*}P < 0.01$, $^{**}P < 0.001$, $^{***}P < 0.0001$ (unpaired *t* test corrected for multiple comparisons using the Holm-Sidak method). Oligo, oligomycin; Rot, rotenone; AA, antimycin A. (**E**) Heatmap, showing the transcriptional profile of mitochondrial genes those related to ox-phos metabolism in AMPKdKO control islets ($P < 0.05$). (**F** and **G**) Morphometric analysis of mitochondria in AMPKdKO and control β cells, showing (**F**) the number of mitochondria per 70 μm^2 ($n = 32–36$), and (**G**) the volume density (mL%). $n = 29–33$ β cells per group. $^{****}P < 0.0001$ (2-tailed unpaired *t* test). (**H**) qPCR, showing the ratio of mtDNA to nuclear DNA in WT adult islets treated with 10 μM compound C (CC) ($n = 3$). $^{***}P = 0.0003$ (2-tailed unpaired *t* test). (**I**) *Ppargc1a* and *Ppargc1b* mRNA levels in the islets of control mice vs. those receiving milk fat throughout their development into adulthood ($n = 3$). MFD, milk fat–supplemented diet. $^{**}P = 0.0013$ (unpaired *t* test corrected for multiple comparisons using the Holm-Sidak method).

mice results in the expression of a transcriptional pattern, including critical genes, that is typical of neonatal islets.

In addition to sharing a transcriptional signature with neonatal β cells, βTSC1-KO islets were also functionally immature. For example, serum insulin levels in βTSC1-KO mice were higher, both after fasting and after glucose stimulation when compared with those of control mice (Supplemental Figure 3D). Correspondingly, βTSC1-KO mice had relatively lower fasting blood glucose levels (mean value of 83 mg/dL in βTSC1 KO vs. 109 mg/dL in control) and cleared injected glucose faster (Supplemental Figure 3, E and F). Furthermore, analysis of dynamic insulin secretion ex vivo showed that βTSC1-KO islets have increased basal insulin secretion at low glucose concentrations but fail to significantly increase this secretion in response to glucose challenge, a behavior seen in immature β cells (Figure 3F).

To further confirm the ability of mTORC1 to elicit an immature phenotype in adult pancreatic β cells, we also crossed *Tsc1*$^{fl/fl}$ mice with those expressing the inducible MIP1-CreER driver in order to generate iTSC1-KO mice (Figure 3G). We first noted that treating adult iTSC1-KO mice with tamoxifen was sufficient to markedly induce p-rpS6 staining among β cells in pancreatic islets (57% stained for p-rpS6), indicative of strong mTORC1 activation (Supplemental Figure 3G). In assessing β cell function we noted that, similar to what was seen in both βTSC1-KO mice and WT mice maintained on dietary milk fat during their entry into adulthood, fasting blood glucose levels were lower after 3 weeks of tamoxifen administration in iTSC1-KO mice than in *Tsc1*$^{fl/fl}$ (no Cre) littermates (Supplemental Figure 3H). Moreover, serum insulin levels were higher, both after fasting and after 30 minutes of glucose stimulation, and injected glucose was correspondingly cleared more rapidly in iTSC1-KO mice versus controls (Figure 3, H and I). Together, these data show that inducing mTORC1 activation in adult β cells is sufficient to spontaneously revert them to an immature, neonatal-type functional state.

AMPK activation triggers a switch to oxidative metabolism in mature islets. In line with data from Yoshihara et al. (3), analysis

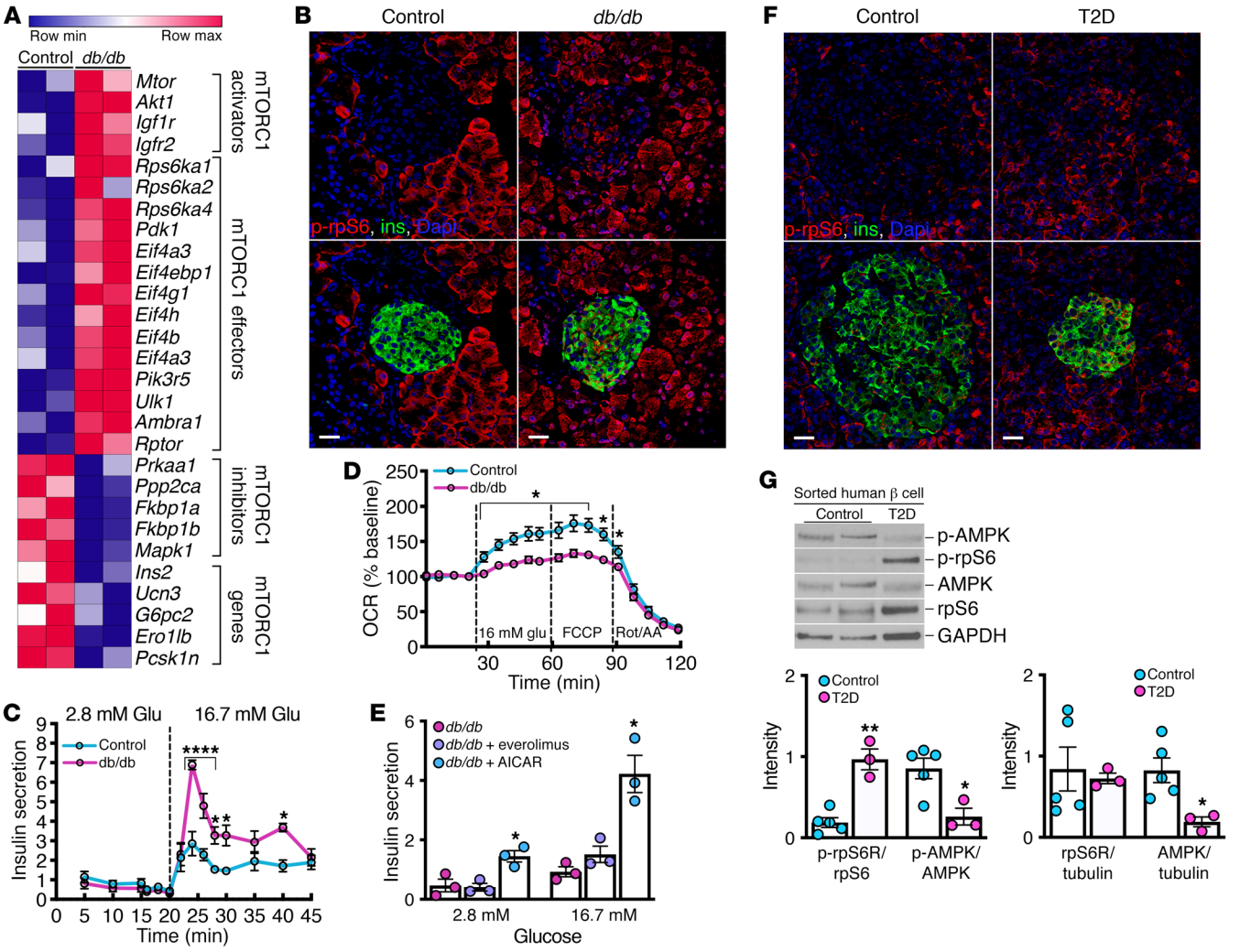

Figure 5. T2D induces increased β cell mTORC1 activity and a reversion of pancreatic islets to an immature phenotype. (**A**) Heatmap, showing the transcriptional profile of genes in the AMPK/mTORC1 pathway and those involved in β cell maturation in islets from *db/db* and control mice ($P < 0.05$). (**B**) Immunostaining for insulin (green) and p-rpS6 (red) in representative pancreatic sections from 4-week-old *db/db* and control mice. Nuclei were counterstained with DAPI (blue). Scale bars: 50 μm. (**C**) Insulin secretion (% of insulin content) in a perifusion assay on islets from 4-week-old *db/db* or control mice in the presence of 2.8 mM and 16 mM glucose ($n = 4$). $^*P < 0.05$, $^{****}P < 0.0001$ (unpaired *t* test corrected for multiple comparisons using the Holm-Sidak method). (**D**) Oxygen consumption rates for *db/db* and control islets presented relative to baseline ($n = 9$–10 per group). Rot, rotenone; AA, antimycin A. $^*P < 0.05$ (unpaired *t* test corrected for multiple comparisons using the Holm-Sidak method). (**E**) GSIS by control and *db/db* islets treated with 40 μM everolimus or 1 mM AICAR ($n = 3$) $^*P < 0.05$ (unpaired *t* test corrected for multiple comparisons using the Holm-Sidak method). (**F**) Immunostaining for insulin (green) and p-rpS6 (red) in representative pancreatic sections from human donors with or without T2D. Nuclei were counterstained with DAPI (blue). Scale bars: 50 μm. (**G**) Representative immunoblots for p-AMPK, p-rpS6, total AMPK, and total rpS6 in healthy donors ($n = 4$) or those with T2D ($n = 3$). GAPDH was used as loading control. Quantifications of p-AMPK and p-rpS6 normalized to total AMPK and rpS6, respectively, and total AMPK or rpS6 normalized to GAPDH are shown below. $^*P < 0.05$, $^{**}P < 0.001$ (unpaired *t* test corrected for multiple comparisons using the Holm-Sidak method).

of our RNAseq data from neonatal and adult pancreatic β cells (Supplemental Figure 1C) revealed an induction of TCA cycle and electron transport chain pathway genes during the transition to adulthood. Intriguingly, 9 out of the total 13 genes encoded by mitochondrial DNA (mtDNA) were upregulated in adult pancreatic β cells during this transition. This included the genes encoding cytochrome *c* oxidase subunits I, II, and III; the NADH dehydrogenases 1, 2, 4, 5, and 6; and the ATP synthase F_0 subunit 6. The expression of other genes, including *Uqcrh*, *Uqcrq*, *Cox5b*, and *Cox6a2*, which are part of the mitochondrial respiratory chain, was also increased in adult versus neonatal pancreatic β cells (Figure 4A). Together, these data suggest that the maturation of pancreatic β cells is orchestrated in conjunction with increased mitochondrial function and oxidative metabolism.

To address the mechanism(s) leading to increased expression of mitochondrial genes, we assessed the ratio of mtDNA copy number per genomic DNA copy number by qPCR. mtDNA copy number in adult islets (mean of 444/cell) was approximately2 times higher than in neonatal ones (mean of 218/cell) (Figure 4B), suggesting that β cell maturation is tied to increased mitochondrial mass. Consistent with this concept, mRNA levels of 2 regulators of mitochondrial biogenesis, *Ppargc1a* (PGC1α)

and *Ppargc1b* (PGC1β), were also higher in adult versus neonatal islets, suggesting that mitochondrial biogenesis is important for β cell maturation (Figure 4C).

Given that the abundance of mtDNA is tightly correlated with cellular respiratory activity (35), we sought to directly assess mitochondrial function by measuring oxygen consumption in neonatal and adult islets using a bioenergetic analyzer (Seahorse XF24). The glucose-stimulated increase in oxygen consumption was markedly higher in isolated adult versus neonatal islets, as was maximal oxygen consumption, which can be measured after treating islets with the mitochondrial uncoupler carbonyl cyanide-4-(trifluoromethoxy)phenylhydrazone (FCCP) (Figure 4D). These data confirm that the increase in β cell mitochondrial mass seen during the transition from neonatal to adult life is commensurate with a pronounced induction of mitochondrial activity.

AMPK activation is known to promote oxidative metabolism (36). We therefore hypothesized that AMPK activation might be responsible for the increase in β cell mitochondrial number and function that we saw during islet maturation. To investigate this possibility, we simultaneously eliminated both AMPK1 and AMPK2 (AMPKdKO) expression selectively in pancreatic β cells by crossing *Prkaa1*$^{fl/fl}$/*Prkaa2*$^{fl/fl}$ mice with Ins-Cre (26) or Rip-Cre (37) mice. RNAseq of islets from adult AMPKdKO (Ins-Cre) and floxed (no Cre) control mice showed that the transcriptomic signatures of AMPKdKO islets were similar to those of WT neonatal islets, importantly including downregulation of the same set of mtDNA-encoded and respiratory pathway genes induced during normal adult β cell maturation (Figure 4E). Monitoring mitochondrial numbers by electron microscopy (EM) confirmed that adult AMPKdKO (Rip-Cre) islets have fewer and smaller mitochondria than those of controls (Figure 4, F and G). We also treated adult islets from WT mice with compound C, an AMPK inhibitor (38) to confirm our findings in AMPKdKO mice. Remarkably, compound C treatment for 24 hours reduced the number of mitochondria in adult islets, recapitulating the knockout phenotype (Figure 4H).

The importance of AMPK regulation during β cell maturation was also evident in our studies with milk fat supplementation. For example, WT mice that continued to consume milk fat throughout the period when weaning normally occurs had lower islet mRNA levels of *Ppargc1a* (no difference for *Ppargc1b*) than did mice weaned onto regular chow in a normal manner (Figure 4I). Taken together, our findings highlight the important role of cellular AMPK activation as a switch that is flipped in response to shifting patterns of macronutrient consumption and that turns on β cell oxidative metabolism, a hallmark of their adult phenotype.

T2D induces increased β cell mTORC1 activity and a reversion of pancreatic islets to an immature phenotype. Insulin resistance, a precursor of T2D, stimulates β cell proliferation in conjunction with hyperinsulinemia (39). Mice lacking functional leptin receptors (*db/db*) are profoundly obese and develop severe, symptomatic hyperglycemia that is often used to model T2D. Notably, *db/db* mice also exhibit a period of compensatory hyperinsulinemia prior to developing overt T2D (40, 41). Given that neonatal islets are also hyperproliferative and display increased insulin secretion, we wondered whether the phenotype of *db/db* mice might involve a reversion of pancreatic β cells back to a relatively immature phenotype. If so, we further wondered whether this reversion could stem from a switch between AMPK and mTORC1 signaling in the opposite direction from that seen during normal β cell maturation.

To test these hypotheses, we performed RNAseq on islets isolated from 4-week-old *db/db* mice and their WT littermates. We found that, in a manner reminiscent of neonatal islets, the expression of mTORC1 activators and mTORC1 effector genes was increased, while the expression of mTORC1 inhibitors and in particular *Prkaa1*, the gene encoding the AMPK α-1 subunit, was repressed in *db/db* islets versus controls (Figure 5A). Moreover, islet immunostaining (p-rpS6 at Ser240/244) showed that mTORC1 activity was higher in β cells from *db/db* mice than control mice (Figure 5B).

To more deeply probe the phenotype of islets in the context of T2D, the transcriptomes of *db/db* and control islets were analyzed using GSEA against a curated list of maturation genes (e.g., *Ins2*, *Ucn3*, *G6pc2*, *Erol1b*, and *Pcsk1n*). Each of these genes was downregulated in *db/db* versus control islets (Figure 5A). Together, these data support the concept that, as hyperglycemia emerges in *db/db* mice, mTORC1 activity increases and AMPK activity falls, leading to the downregulation of genes normally expressed in functionally mature β cells. These observations point to T2D as being a state characterized by a reversion of β cells towards an immature phenotype. Consistent with this view, *db/db* islets secreted more insulin than control islets (Figure 5C) and had both lower glucose-stimulated and maximal oxygen consumption rate (OCR) than did control islets, indicating reduced oxidative respiratory capacity in line with downregulated AMPK activity (Figure 5D).

To further explore the roles of AMPK and mTORC1 in diabetic islets, we used both everolimus and AICAR to modulate the activity of AMPK and mTORC1, respectively, in *db/db* islets from 12-week-old mice, and then assessed GSIS. Inhibiting mTORC1 with everolimus had no effect on insulin secretion from *db/db* mouse islets. By contrast, repressing mTORC1 activity by activating AMPK with AICAR resulted in enhanced insulin secretion at both 2.8 mM and 16.7 mM extracellular glucose (Figure 5E).

We also examined whether the relationship between mTORC1 and AMPK in islets translated to human subjects, including healthy individuals and those with T2D. Immunostaining for p-rpS6 (Ser240/244) revealed increased mTORC1 activation in islets from individuals with T2D (Figure 5F), a reactivation consistent with reversion to an immature phenotype, and matching observations in islets from *db/db* mice. We simultaneously assessed mTORC1 activation in isolated β cells sorted as previously described (42) from islets dispersed from the pancreata of healthy subjects and those with T2D. Immunoblots of this β cell–enriched population showed that whereas total rpS6 levels were similar between control samples and those from individuals with T2D, levels of p-rpS6 (Ser240/244) were increased in the context of T2D, mirroring what was seen by islet immunostaining. We similarly assessed activation of AMPK in sorted β cells and found that although there was less total AMPK in the context of T2D (P = 0.045, n = 3), levels of p-AMPK (Thr172) were specifically reduced as well (Figure 5G). These data reveal what we believe is a new mechanism, involving reactivation of a neonatal signaling pattern in β cells, that underlies β cell dysfunction in T2D spanning from mouse models to human subjects. Indeed, we show that islets from individuals with T2D are characterized by relative mTORC1 activation and AMPK inhibition.

Discussion

β Cell maturation entails the acquisition of GSIS capability and a loss of proliferative capacity. The principal aims of this study were to explore what governs these dynamic changes, an important issue given that a reversal of functional β cell maturity may contribute to deficient glucose responsiveness in T2D (43) and, conceivably, to the failure of residual β cells in type 1 diabetes (44). We show using multiple approaches that a switch from mTORC1- to AMPK-dependent signaling in β cells controls this process, both in mice and humans.

Relative mTORC1 activation in neonatal islets is associated with β cell proliferation and constitutive insulin secretion, as compared with less proliferative and more specifically glucose-responsive adult islets. Remarkably, artificially reactivating mTORC1 in adult islets could recapitulate the neonatal phenotype, as it was sufficient to both reduce the expression of maturity-defining β cell genes and impair normal GSIS. Others have demonstrated a similar effect by activating mTORC1 via β cell–selective deletion of Raptor, which also decreases β cell mass and size, and reduces GSIS (18).

Our work probing the TSC1/2 complex in β cells further supports the importance of mTORC1 signaling in maintaining β cell immaturity. Importantly, these findings also agree with data from earlier studies (9, 10, 14, 45). For example, constitutively activating mTORC1 signaling by inactivating TSC1 or TSC2 leads to an expansion of β cell mass via enhanced cell division (14) and hypertrophy (10, 46).

Our ability to induce an mTORC1-dependent subsidence of normal GSIS may involve altered expression of genes involved in glucose sensing, for example upregulation of the low-K_M hexokinase (HK1) and derepression of disallowed genes including *Ldha*, in line with previous reports (26, 47). Such alterations would enhance glycolytic ATP generation, leading to closure of ATP-sensitive K^+ channels and constitutive insulin release even at low extracellular glucose levels (30). Inducing mTORC1-dependent β cell immaturity may also compromise both triggering (48) and amplifying (49, 50) pathways needed for appropriate GSIS in response to increasing extracellular glucose levels. The consequence of this mTORC1-driven regime is to prompt basal insulin secretion but impair glucose responsiveness.

This all indicates that a repression of mTORC1-dependent signaling is required to license β cells to undergo transcriptional and functional maturation. We show here that AMPK, a known inhibitor of mTORC1 in other contexts, is responsible for exerting this repressive effect. Indeed, prior work showed a tight reciprocal relationship between AMPK activity and mTORC1 signaling in clonal mouse β cells (51). Moreover, deleting the upstream AMPK kinase LKB1 markedly increases mTORC1 signaling in islets, an effect likely due, at least in part, to AMPK inhibition (24, 25). Although we show ample evidence supporting the reciprocal relationship between AMPK and mTORC1 in maturing β cells here, we did not clearly see increased mTORC1 signaling in islets from mice lacking both AMPK α subunits (results not shown). However, this probably reflects effects related to deleting AMPK chronically and during development.

Beyond its direct effect of modulating the phosphorylation state of mTORC1 (11), AMPK may potentiate β cell maturation in other ways as well. For example, AMPK may act to repress the expression of disallowed genes (26). Although the precise mechanism by which this might occur is unknown, there is evidence suggesting that AMPK can regulate β cell miR levels (26, 27) and potentially induce epigenetic changes that alter chromatin accessibility at relevant genomic loci (unpublished data).

Importantly, several of the phenotypic features of immaturity inducible in β cells and islets by forcing either mTORC1 activation or AMPK inhibition could be reproduced by maintaining high milk fat consumption in mice emerging from the neonatal period. Indeed, our data support the concept that AMPK activation and consequent mTORC1 inhibition among β cells during the transition from neonatal to adult life are driven by specific shifts in macronutrient consumption that take place when animals wean from near-constant consumption of a relatively high-fat-milk diet and begin to consume a mixed diet that is relatively carbohydrate-rich in a diurnally recurring manner. This dietary shift might significantly lower the time-averaged intracellular ATP versus ADP/AMP ratios in β cells due to decreased overall oxidative flux through the TCA cycle. Such a reduction would be expected to activate AMPK via both well-defined posttranslational modifications (phosphorylation of α subunits at Thr172) and potentially by other transcriptional and/or translational mechanisms.

We also show that AMPK activation in adult islets likely promotes mitochondrial biogenesis, as mitochondrial genes (and nuclear-encoded genes involved in mitochondrial function) were clearly repressed in AMPKdKO mouse islets. This repression correlates with the concomitant reduction we observed in ATP generation via oxidative phosphorylation.

Other changes concomitant with β cell maturation include a characteristic shift in islet polarization, islet compaction, and their organization into rosette-like structures around islet capillaries, concordant with their ability to sense glucose and secrete appropriate amounts of insulin into the blood (52). These changes occur during the postnatal period, increase significantly by P11, and reach a maximum during the entry into adulthood (53).

The Wnt/planar cell polarity (PCP) pathway, conserved across mammals, regulates islet polarity and compaction, through its effector Flattop, to promote β cell maturation and function (53). The ratios of Flattop-negative to Flattop-positive β cells are similar to the ratios we quantified for p-rpS6–positive to –negative β cells, suggesting that the process driving islet polarization and compaction may be linked to the β cell mTORC1-to-AMPK signaling switch we highlight. Interestingly, LKB1/AMPK signaling is known to be important in establishing pancreatic β cell polarity. For example, deleting LKB1, an AMPK activator, leads to the inappropriate positioning of nuclei around capillaries, and altered localization of cilia at the center of rosettes (24). Thus, mTORC1-AMPK switching may orchestrate multiple interconnected aspects of β cell and islet maturation.

Our findings indicate, strikingly, that mTORC1 activation in models of T2D (mouse and human) may both initiate and drive changes in β cell signaling, phenotype, and function that are part of both the transient compensatory response to systemic insulin resistance, as well as the subsequent deterioration that ultimately produces T2D. Indeed, mTORC1 activation was increased in islets of both *db/db* mice and human subjects with T2D, when compared with relevant controls. Similar findings were recently reported by Yuan et al., who observed a decrease in mTORC2 activation in islets from

diabetic subjects (54). The former studies, however, did not provide any insights into the regulation of mTORC1 or mTORC2 activity.

We suggest that lowered AMPK activity is likely to be a major driver of increased mTORC1 signaling in T2D islets, driving β cells to a more immature state. Indeed, previous work (55) reported lowered AMPK activation in T2D islets, although specific reductions in levels of AMPK α subunits was not observed. Likewise, Solimena et al. (56) report that AMPK and insulin/IGF-1 signaling in islets are specifically affected in people with T2D, using laser capture microdissection to show changes in pancreatic mRNA levels of both *PRKAB2* (AMPKβ2) and *PRKAG2* (AMPKγ2).

How AMPK activity is reduced in T2D remains an open question. When measured in vitro at equal glucose concentrations, glucose oxidation is lowered in the islets of those with T2D versus those of control subjects (55). This is somewhat puzzling, as the hyperglycemia characterizing T2D might be expected to increase metabolic flux in β cells and, in turn, increase intracellular ATP/ADP and ATP/AMP ratios, which is not what has been reported. At any rate, altered energetic flux likely underlies the reduction in phosphorylation of catalytic AMPK α subunits that takes place in the context of T2D. Resolving this issue will require precise measurements of adenine nucleotides, as well as the activity of other AMPK regulators including the relevant upstream kinases and phosphatases (22) in T2D β cells.

Our study provides comprehensive evidence indicating that mTORC1 and AMPK form a reciprocally coupled switch that is controlled by metabolic and nutritional factors and that is central to the maturation of the pancreatic β cell. Remarkably, this same switch becomes defective, operating in a reverse direction and promoting β cell immaturity and consequent functional impairment in T2D. Therapeutic approaches to stimulate AMPK activity in the β cell may thus provide valuable new tools to improve insulin output in this disease, complementing the recently reported actions of such drugs in insulin-sensitive tissues (57, 58).

Methods

Mouse studies. MIP-GFP [B6.Cg-Tg(Ins1-EGFP)1Hara/J] mice were used to sort pancreatic β cells and perform RNAseq on a pure pancreatic β cell population. C57BL/6J mice were used to assess pancreatic β cell maturation and confirm the data obtained from RNAseq. βTSC1-KO and iTSC1-KO mice were generated by crossing Rip-Cre mice [B6N.Cg-Tg(Ins2-Cre)25Mgn/J] and MIP1-CreER [B6.Cg-Tg(Ins1-Cre/ERT)1Lphi/J] mice, respectively, with mice expressing conditional alleles of *Tsc1*$^{fl/fl}$ (*Tsc1*$^{fl/fl}$; Tsc1tm1Djk/J). AMPKdKO mice were generated as previously described (26, 37). All these mice, including *db/db* mice (BKS.Cg-Dock7m$^{+/+}$ Leprdb/J), were purchased from The Jackson Laboratory.

MIP-GFP and Rip-Cre mice express a human growth hormone (hGH) minigene (59), a fact that could cause confusion when interpreting results obtained using either model. To avoid confounds and associated ambiguity in our data analysis, we used a series of controls to confirm the validity of the data we obtained using both MIP-GFP and Rip-Cre mice. MIP-GFP mice were used to facilitate sorting of pancreatic β cells, and thus simplify performing RNAseq on a highly pure β cell population. Note that because we compared neonatal versus adult MIP-GFP mice, both groups had β cells expressing the same minigene. Thus we compared between chronological ages while spreading the impact, if any, of the minigene evenly across groups. This fact reduces the likelihood that any differences we observed were due to the presence of the hGH minigene per se.

We further confirmed the validity of the RNAseq data obtained using MIP-GFP mice in C57BL/6J mice, which do not express the minigene at all. For example, the RNAseq data obtained from the β cells of MIP-GFP mice supported a relative activation of mTORC1 in neonatal pancreatic β cells and relative activation of AMPK in adult β cells. Each of these findings were rigorously confirmed in C57BL/6J mice by immunofluorescence histology, β cell FACS, and immunoblot.

Moreover, the RNAseq experiment on MIP-GFP β cells revealed a switch in cellular metabolism and an increase in the expression of mitochondrial genes. We confirmed these data too by assessing mitochondrial number, the relative mRNA levels of *Ppargc1a* and *Ppargc1b*, and cellular oxygen consumption all independently in islets from C57BL/6J mice. Taken together, these controls offer considerable evidence to support the contention that our findings in β cells using the MIP-GFP model are not a consequence of the hGH minigene in the construct used to make the mice.

Rip-Cre mice were used for crossing with *Tsc1*$^{fl/fl}$ mice to generate Rip-Cre–dependent TSC1-deficient mice (βTCS1-KO mice). However, in our studies, we compared *Tsc1*$^{fl/fl}$ mice (Cre-negative), Rip-Cre mice (no flox), and βTSC1-KO mice (Cre^{+}). In this comparison, we found no differences between mice that expressed TSC1 but either did (Rip-Cre, no flox) or did not (*Tsc1*$^{fl/fl}$) express the hGH minigene. As such, we can confidently conclude that the differences we found are due to the forced activation of mTORC1, and not due to off-target effects resulting from the minigene. Moreover, we also used a completely separate inducible Cre model (MIP1-CreER), which does not express the hGH minigene, to activate mTORC1 in adult mice (iTSC1 KO). iTSC1-KO mice (no minigene) had a phenotype similar to the one seen in βTCS1-KO mice, which expressed the minigene. Rip-Cre mice were also used to generate AMPKdKO mice in order to assess the number of mitochondria per β cell area, and mitochondrial volume density per β cell. The controls used in these experiments are heterozygous mice (*Prkaa1*$^{+/fl}$/*Prkaa2*$^{+/fl}$; Rip-Cre^{+}) in order to again spread the presence of the hGH minigene equally across groups.

Mice were fed ad libitum and housed under a 12-hour light/12-hour dark cycle. Genotyping was performed by Transnetyx on tail snips using a PCR-based protocol. For tamoxifen-inducible mice, we injected adult mice (8 weeks old) with 75 mg/kg of tamoxifen i.p. for 5 consecutive days.

In order to maintain milk fat as a principal source of nutrients and to reduce consumption of carbohydrates, Newborn pups (males and females) were provided oral milk fat (1% v/w) or vehicle by daily gavage beginning at P11–P13 while remaining with their nursing mothers in the presence of dietary pellets containing 42% of calories from milk fat (Western diet). At P21, control pups were weaned on a standard rodent chow diet with vehicle gavage, whereas the milk-fat group was weaned onto a Western diet while continuing to receive daily milk fat gavage. All mice were maintained in this manner until they were analyzed at P40.

Metabolic and physiological analyses. Fasting blood glucose concentrations in mice were determined using a handheld glucometer (Freestyle Lite) after 6 hours of fasting. For in vivo glucose challenges, mice were fasted for 6 hours, after which serum insulin and blood glucose were collected by submandibular bleeding prior to and 30 minutes following an i.p. injection of glucose (2 g/kg); serum was collected by centrifugation and insulin levels measured by ELISA (Mercodia). For glu-

cose tolerance tests, blood glucose levels were measured before, and 15, 30, 60, and 120 minutes following an i.p. injection of glucose (2 g/kg).

An automated perifusion system (BioRep Technologies) was used to measure dynamic insulin secretion by islets. Twenty to 30 size-matched islets per mouse were immobilized in Bio-Gel P-4 Gel (Bio-Rad) that was maintained at 37°C in a temperature-controlled chamber. Islets were perifused at 100 μL/min with Krebs-Ringer bicarbonate buffer supplemented with 0.25% BSA (KRB buffer) and containing 2.8 mM glucose for a preincubation period of 30 minutes. Islets were next perifused in sequence with KRB buffer containing 2.8 mM glucose for 20 minutes, following by KRB buffer containing 16.7 mM glucose for 30 minutes, and finally KRB buffer containing 30 mM KCl for 10 minutes. Flow-through was collected every minute during the 3 perifusion steps of the assay. Islets were next recovered from the chambers and insulin content was extracted by overnight incubation in acid/ethanol solution. For static measurements of GSIS by *db/db* islets, the newly isolated islets were first incubated overnight in medium with 11 mM glucose, after which they were preincubated in KRB buffer containing 2.8 mM glucose with or without 1 mM AICAR or 40 μM everolimus for 1 hour. The islets were next incubated in KRB buffer containing 2.8 mM glucose for 30 minutes, 16.7 mM glucose for another 30 minutes, and then KCl as above, with respective AICAR or everolimus treatment maintained during steps. The supernatant was collected after each incubation. Total insulin content was then extracted from islets by overnight incubation with acid/ethanol solution. Insulin in the supernatants and islet extracts was then measured by ELISA.

Flow cytometry and β cell sorting. Islets from neonatal (P6) or postweaning (P45) mice were dissociated, fixed, permeabilized, and stained for p-rpS6 and insulin (5018 or 9008, respectively, Cell Signaling Technology) for FACS analysis using a BD LSRFortessa X20 Dual machine. FACS data were analyzed with FlowJo software.

Islets from MIP-GFP mice were digested into a single-cell suspension and sorted for GFP by FACS to 85%–95% average purity. Sorted cells were then processed for RNA extraction.

Human islet samples were obtained from both healthy adult organ donors and adult donors with T2D. Islets were dissociated using Accumax (STEMCELL Technologies) for 7–8 minutes and washed 3 times with PBS containing 2% BSA and 2.8 mM glucose. Cells were next incubated for 30 minutes at 4°C in the presence of the pancreatic marker antibodies HPi2 (77-HPI2-PU-0.1, clone HIC1-2B4, ALPCO) and HPa3 (provided by Markus Grompe, Oregon Health Sciences University, Portland, Oregon, USA). After washing, samples were incubated at room temperature for an additional 30 minutes in the presence of fluorescent-coupled secondary antibodies. Cells were next washed and resuspended in PBS containing 2% BSA and 2.8 mM glucose. Before sorting, DAPI stain was added to distinguish live versus dead cells. The details of the gating strategy are shown in Supplemental Figure 4A.

Transmission EM analysis. Pancreatic islets (~30) were fixed in 2.5% (w/v) glutaraldehyde in PBS at 4°C. After being washed in PBS, islets were postfixed in 0.1% (w/v) osmium tetroxide in PBS and dehydrated in a graded series of ethanol. The islets were then rapidly transferred to propylene oxide and embedded in PolyBed 812 (Polysciences, Inc).

Ultrathin sections were cut with a diamond knife, stained with uranyl acetate and lead citrate, and observed under a Zeiss 902 transmission electron microscope. β Cells were identified under EM by their distinct morphology including dense core granules (60). β Cells were considered dead based on a loss of plasma membrane integrity, fragmentation into discrete bodies, or engulfment of the cell corpse or its fragments by an adjacent cell (61). The presence of marked chromatin condensation and/or of blebs was considered signs of apoptosis, whereas massive vacuole accumulation and absence of chromatin condensation were considered signs of autophagy (62).

For morphometric studies, volume density values were derived from the evaluation of 3–5 different islets for each pancreas. Twelve photomicrographs were taken of each islet at $\times 10^5$ magnification. A graticule (11 × 11 cm) composed of 169 points was placed on the micrographs, and the number of points intersecting the autophagic vacuoles and mitochondria was counted. Volume density of intracellular organelles was calculated according to the formula VD = Pi/Pt, where Pi is the number of points within the subcellular component and Pt is the total number of points within the cells, and expressed in mL/100 mL of tissue (mL%) (63).

Assessments of cellular metabolism and mitochondrial number. The OCR of β cells was measured in real time using a Seahorse XF24 analyzer (Seahorse Bioscience). Batches of 30 islets were loaded into islet-capture microplates and covered with a mesh to prevent movement of the islets during the assay. This was followed by incubation in a non-CO_2 incubator at 37°C for 1 hour. Three to 5 measurements in 2.8 mM glucose were taken, followed by replacement with 16.7 mM glucose and sequential addition of 5 μM oligomycin (Cell Signaling Technology, 9996L), 1 μM FCCP (C2920-10mg), 5 μM rotenone (R8875-1G), and 5 μM antimycin A (A8674-50MG) (all 3 from Sigma-Aldrich). OCR was normalized to the average baseline measurement in 2.8 mM glucose, and expressed as a percentage change from this baseline during the assay. After the experiment, the islets underwent DNA extraction, and the number of mitochondria was determined by qPCR as a ratio of mtDNA copy number per genomic DNA copy number using the following primers. For mtDNA: forward, GAGCATCTTATCCACGCTTCC; reverse, GGTGGTACTCCCGCTGTAAA. For genomic DNA: forward, CTTCCCCACTGGCCTCAAG; reverse, CCAAAACCCAGTGATCCAGC.

Immunofluorescence staining and morphometric analysis of islets. A standard immunofluorescence protocol was performed to stain paraffin sections of fixed human and mouse pancreata using the following primary antibodies: anti–p-Ser240/244-rpS6 (5364, Cell Signaling Technology), anti–p-Thr172-AMPK (2535S, Cell Signaling Technology,) anti-insulin (A056401-2, Agilent), anti-Pdx1 (F109-D12, Developmental Studies Hybridoma Bank), and anti-MafA (NBP1-00121, Novus Biologicals). Briefly, pancreatic tissue was flushed with PBS, dissected, fixed in buffered zinc formalin fixative (Z-Fix, Anatech Ltd) overnight, dehydrated in grades of ethanol, and processed for paraffin embedding. Sections (5 μm) were heated, de-waxed, rehydrated through a series of ethanol dilutions, and then placed in distilled H_2O. Heat-induced epitope retrieval was performed by immersion in antigen unmasking solution (H-3300, Vector) and microwave heating. After blocking with antibody diluent (DAKO), sections were incubated with a primary antibody and then with appropriate Alexa Fluor 488– or 555–coupled secondary antibodies (Jackson ImmunoResearch). Nuclei were counterstained using DAPI. To stain with anti–p-AMPK (Thr172), PBS-flushed pancreata were perfused in vivo with 4% paraformaldehyde (PFA) via intracardiac catheter prior to dissection in order to fix the pancreas as quickly as possible. The pancreata were then dissected and incubated for 2 hours in 4% PFA and then conserved in OCT at –80°C until sectioning. Cryosections were then

washed with PBS followed by the antigen retrieval and blocking steps as described above.

RNA isolation, RT-PCR, and real-time PCR. RNA was isolated using Direct-zol (Zymo Research) and digested with RNase-free DNase to eliminate DNA. RNA (50–200 ng) was used for preparation of cDNA using Superscript IV Reverse Transcriptase (Invitrogen) by the oligo(dT) priming method. qPCR was performed using the 1× Fast SYBR Green Mix (Applied Biosystems) in an ABI7900HT system (Applied Biosystems). The expression levels of each transcript were normalized to the housekeeping gene RPLP19. The primer sequences used are listed in Supplemental Table 7.

RNAseq library generation. For neonatal versus adult, βTSC1 KO versus control, and *db/db* versus control RNAseq analyses, total RNA was isolated from the appropriate preparation using Direct-zol RNA MicroPrep plus (Zymo Research), following the manufacturer's instructions. Sequencing libraries were prepared from 10–25 ng of total RNA using the SMARTer Stranded RNAseq Kit (Clontech) according to the manufacturer's protocol. Briefly, after rRNA depletion, remaining RNA was used for first-strand cDNA synthesis and purification, after which the samples were ligated to unique adapters and PCR amplified. Libraries were then validated using a 2100 Bio-Analyzer (Agilent), normalized, and pooled for sequencing using the UCSF Institute for Human Genetics core service.

To process RNAseq libraries, adaptor sequences were trimmed using Cutadapt version 1.13 (64), requiring a length greater than 20 nt after trimming, and quality filtered by requiring all bases to have a minimum score of 20 (-m 20 -q 20). Only reads that passed the quality or length threshold on both strands were considered for mapping. Reads were mapped with the spliced-read mapper GSNAP (version 2016-08-10) (65) using default parameters. Reads were aligned against the NCBIM37 (mm9) genome build release 67 downloaded from Ensemble. Reads mapping to the genes of interest were counted using HTseq (v.0.7.1) (66) in the union mode. Differential expression analysis was performed in R using DESeq2 (v.1.16.0) (67) with the default parameters, including the Cook's distance treatment to remove outliers. AMPKdKO RNAseq data were obtained as previously described (26).

RNAseq data that support the findings of this study have been deposited in the NCBI's Gene Expression Omnibus (GEO) under accession code GSE132261. From Kone et al., data for RNAseq are available at the European Molecular Biology Laboratory–European Bioinformatics Institute (EMBL-EBI) ArrayExpress website under accession number E-MTAB-2791.

Immunoblotting. Cells were lysed in ice-cold RIPA buffer containing a cocktail of protease and phosphatase inhibitors. Lysates were kept on ice for 5 minutes and cleared by centrifugation. Protein concentrations were determined using the Pierce 660nm Protein Assay, and immunoblotting was performed using the Bolt mini-gel and iBlot2 system. Membranes were next blocked with 5% BSA and incubated overnight with primary antibodies anti–p-rpS6 (Ser240/244, 1:1000, 5364), anti–p-AMPK (Ser172, 1:1000, 2535S), anti-rpS6 (2217S, 1:1000), anti-AMPK (5831S, 1:1000) (all from Cell Signaling Technology), and anti–β-tubulin (ab11307, 1:5000) and anti-GAPDH (ab8245, 1:5000) from Abcam. Primary incubation was followed by a 1-hour incubation with the secondary antibody at room temperature, after which the blots were revealed using the ECL system. We routinely used both GAPDH and tubulin as loading controls. Rarely, as was the case for the data presented in Figure 5G, we were unable to effectively blot for β-tubulin. In this case, GAPDH served as the sole loading control.

Statistics. Statistical analyses performed for specific data sets are described in the figure legends. All statistical tests were performed using GraphPad Prism software v8. Data are presented as mean ± SEM and were subjected to 2-tailed unpaired Student's *t* test. For multiple comparisons, unpaired *t* tests were corrected using the Holm-Sidak method. Significance was assessed using *P*-value cutoffs indicated as follows: $^{*}P < 0.05$, $^{**}P < 0.01$, $^{***}P < 0.001$, and $^{****}P < 0.0001$.

Study approval. All animal experiments were performed in accordance with NIH policies on the use of laboratory animals and approved by the UCSF Institutional Animal Care and Use Committee (IAAUC).

Author contributions

RJ, ST, GAR, SKK, and AB conceived of and designed the research. RJ, ST, ANS, GS, MM, MV, and AS performed the experiments. RJ, ST, SG, PM, MM, ANS, AM, MH, YD, GAR, SKK, and AB analyzed the data and interpreted the results. RJ, SKK, and AB prepared the figures and drafted the manuscript. RJ, ST, ANS, GS, PM, MM, AS, SG, EBM, AM, MH, YD, GAR, SKK, and AB edited and revised the manuscript. All authors reviewed the final manuscript. Authorship order between AB and SKK was determined based on greater responsibility for funding the project, including support for other authors contributing to the study.

Acknowledgments

GAR was supported by a Wellcome Trust Senior Investigator (WT098424AIA) and Investigator Award (212625/Z/18/Z), by MRC Programme grants (MR/R022259/1, MR/J0003042/1, MR/L020149/1, and MR/R022259/1), an Experimental Challenge Grant (DIVA, MR/L02036X/1), and Project grants from the MRC (MR/N00275X/1), and Diabetes UK (BDA/11/0004210, BDA/15/0005275, and BDA 16/0005485). YD was supported by grants from the Human Islet Research Network (HIRN) and the DON foundation. This project was also supported by NIH/NIDDK grants, including DK108666 to MH, DK103175 and DK112304 to SKK, a Diabetes Research Center P30 grant (DK063720), and a Nutrition and Obesity Research Center P30 grant (DK098722).

Address correspondence to: Suneil K. Koliwad or Anil Bhushan, Diabetes Center, 513 Parnassus Avenue, San Francisco, California 94143, USA. Phone: 415.476.9623; Email: suneil.koliwad.ucsf.edu (S.K. Koliwad). Phone: 415.502.3295; Email: bhushan.lab@ucsf.edu (A. Bhushan).

1. Blum B, Hrvatin S, Schuetz C, Bonal C, Rezania A, Melton DA. Functional beta-cell maturation is marked by an increased glucose threshold and by expression of urocortin 3. *Nat Biotechnol*. 2012;30(3):261–264.
2. Dhawan S, et al. DNA methylation directs functional maturation of pancreatic β cells. *J Clin Invest*. 2015;125(7):2851–2860.
3. Yoshihara E, et al. ERRγ is required for the metabolic maturation of therapeutically functional glucose-responsive β cells. *Cell Metab*. 2016;23(4):622–634.
4. Alejandro EU, et al. Maternal diet-induced microRNAs and mTOR underlie β cell dysfunction in offspring. *J Clin Invest*. 2014;124(10):4395–4410.
5. Jacovetti C, Matkovich SJ, Rodriguez-Trejo A, Guay C, Regazzi R. Postnatal β cell maturation is

associated with islet-specific microRNA changes induced by nutrient shifts at weaning. *Nat Commun*. 2015;6:8084.
6. Stolovich-Rain M, et al. Weaning triggers a maturation step of pancreatic β cells. *Dev Cell*. 2015;32(5):535–545.
7. Aguayo-Mazzucato C, et al. Mafa expression enhances glucose-responsive insulin secretion in neonatal rat beta cells. *Diabetologia*. 2011;54(3):583–593.
8. Gu C, et al. Pancreatic beta cells require NeuroD to achieve and maintain functional maturity. *Cell Metab*. 2010;11(4):298–310.
9. Balcazar N, et al. mTORC1 activation regulates beta-cell mass and proliferation by modulation of cyclin D2 synthesis and stability. *J Biol Chem*. 2009;284(12):7832–7842.
10. Mori H, et al. Critical roles for the TSC-mTOR pathway in β cell function. *Am J Physiol Endocrinol Metab*. 2009;297(5):E1013–E1022.
11. Saxton RA, Sabatini DM. mTOR signaling in growth, metabolism, and disease. *Cell*. 2017;169(2):361–371.
12. Alejandro EU, et al. Overexpression of kinase-dead mTOR impairs glucose homeostasis by regulating insulin secretion and not β cell mass. *Diabetes*. 2017;66(8):2150–2162.
13. Elghazi L, Blandino-Rosano M, Alejandro E, Cras-Méneur C, Bernal-Mizrachi E. Role of nutrients and mTOR signaling in the regulation of pancreatic progenitors development. *Mol Metab*. 2017;6(6):560–573.
14. Rachdi L, et al. Disruption of Tsc2 in pancreatic beta cells induces beta cell mass expansion and improved glucose tolerance in a TORC1-dependent manner. *Proc Natl Acad Sci U S A*. 2008;105(27):9250–9255.
15. Shigeyama Y, et al. Biphasic response of pancreatic beta-cell mass to ablation of tuberous sclerosis complex 2 in mice. *Mol Cell Biol*. 2008;28(9):2971–2979.
16. Blandino-Rosano M, et al. Loss of mTORC1 signalling impairs β cell homeostasis and insulin processing. *Nat Commun*. 2017;8:16014.
17. Chau GC, et al. mTOR controls ChREBP transcriptional activity and pancreatic β cell survival under diabetic stress. *J Cell Biol*. 2017;216(7):2091–2105.
18. Ni Q, et al. Raptor regulates functional maturation of murine beta cells. *Nat Commun*. 2017;8:15755.
19. Hardie DG, Schaffer BE, Brunet A. AMPK: an energy-sensing pathway with multiple inputs and outputs. *Trends Cell Biol*. 2016;26(3):190–201.
20. Gwinn DM, et al. AMPK phosphorylation of raptor mediates a metabolic checkpoint. *Mol Cell*. 2008;30(2):214–226.
21. Inoki K, Zhu T, Guan KL. TSC2 mediates cellular energy response to control cell growth and survival. *Cell*. 2003;115(5):577–590.
22. Hardie DG. AMP-activated protein kinase: an energy sensor that regulates all aspects of cell function. *Genes Dev*. 2011;25(18):1895–1908.
23. Fu A, et al. Loss of Lkb1 in adult beta cells increases beta cell mass and enhances glucose tolerance in mice. *Cell Metab*. 2009;10(4):285–295.
24. Granot Z, et al. LKB1 regulates pancreatic beta cell size, polarity, and function. *Cell Metab*. 2009;10(4):296–308.
25. Sun G, et al. LKB1 deletion with the RIP2.Cre transgene modifies pancreatic beta-cell morphology and enhances insulin secretion in vivo. *Am J Physiol Endocrinol Metab*. 2010;298(6):E1261–E1273.
26. Kone M, et al. LKB1 and AMPK differentially regulate pancreatic β cell identity. *FASEB J*. 2014;28(11):4972–4985.
27. Martínez-Sánchez N, et al. Hypothalamic AMPK-ER stress-JNK1 axis mediates the central actions of thyroid hormones on energy balance. *Cell Metab*. 2017;26(1):212–229.e12.
28. Subramanian A, et al. Gene set enrichment analysis: a knowledge-based approach for interpreting genome-wide expression profiles. *Proc Natl Acad Sci U S A*. 2005;102(43):15545–15550.
29. Wittenberg AD, et al. Phosphorylated ribosomal protein S6 is required for Akt-driven hyperplasia and malignant transformation, but not for hypertrophy, aneuploidy and hyperfunction of pancreatic β cells. *PLoS ONE*. 2016;11(2):e0149995.
30. da Silva Xavier G, Leclerc I, Varadi A, Tsuboi T, Moule SK, Rutter GA. Role for AMP-activated protein kinase in glucose-stimulated insulin secretion and preproinsulin gene expression. *Biochem J*. 2003;371(Pt 3):761–774.
31. Salt IP, Johnson G, Ashcroft SJ, Hardie DG. AMP-activated protein kinase is activated by low glucose in cell lines derived from pancreatic beta cells, and may regulate insulin release. *Biochem J*. 1998;335(Pt 3):533–539.
32. Brissova M, et al. Assessment of human pancreatic islet architecture and composition by laser scanning confocal microscopy. *J Histochem Cytochem*. 2005;53(9):1087–1097.
33. Godbole VY, Grundleger ML, Pasquine TA, Thenen SW. Composition of rat milk from day 5 to 20 of lactation and milk intake of lean and preobese Zucker pups. *J Nutr*. 1981;111(3):480–487.
34. Pullen TJ, Huising MO, Rutter GA. Analysis of purified pancreatic islet beta and alpha cell transcriptomes reveals 11β-hydroxysteroid dehydrogenase (Hsd11b1) as a novel disallowed gene. *Front Genet*. 2017;8:41.
35. D'Erchia AM, et al. Tissue-specific mtDNA abundance from exome data and its correlation with mitochondrial transcription, mass and respiratory activity. *Mitochondrion*. 2015;20:13–21.
36. Marcinko K, Steinberg GR. The role of AMPK in controlling metabolism and mitochondrial biogenesis during exercise. *Exp Physiol*. 2014;99(12):1581–1585.
37. Sun G, et al. Ablation of AMP-activated protein kinase alpha1 and alpha2 from mouse pancreatic beta cells and RIP2.Cre neurons suppresses insulin release in vivo. *Diabetologia*. 2010;53(5):924–936.
38. Bain J, et al. The selectivity of protein kinase inhibitors: a further update. *Biochem J*. 2007;408(3):297–315.
39. Cerf ME. Beta cell dynamics: beta cell replenishment, beta cell compensation and diabetes. *Endocrine*. 2013;44(2):303–311.
40. Coleman DL, Hummel KP. Hyperinsulinemia in pre-weaning diabetes (db) mice. *Diabetologia*. 1974;10(Suppl):607–610.
41. Dubuc PU. The development of obesity, hyperinsulinemia, and hyperglycemia in ob/ob mice. *Metab Clin Exp*. 1976;25(12):1567–1574.
42. Dorrell C, Abraham SL, Lanxon-Cookson KM, Canaday PS, Streeter PR, Grompe M. Isolation of major pancreatic cell types and long-term culture-initiating cells using novel human surface markers. *Stem Cell Res*. 2008;1(3):183–194.
43. Talchai C, Xuan S, Lin HV, Sussel L, Accili D. Pancreatic β cell dedifferentiation as a mechanism of diabetic β cell failure. *Cell*. 2012;150(6):1223–1234.
44. Rui J, Deng S, Arazi A, Perdigoto AL, Liu Z, Herold KC. β Cells that resist immunological attack develop during progression of autoimmune diabetes in NOD mice. *Cell Metab*. 2017;25(3):727–738.
45. Ding L, Yin Y, Han L, Li Y, Zhao J, Zhang W. TSC1-mTOR signaling determines the differentiation of islet cells. *J Endocrinol*. 2017;232(1):59–70.
46. Anzi S, et al. Postnatal exocrine pancreas growth by cellular hypertrophy correlates with a shorter lifespan in mammals. *Dev Cell*. 2018;45(6):726–737.e3.
47. Yavari A, et al. Chronic activation of γ2 AMPK induces obesity and reduces β cell function. *Cell Metab*. 2016;23(5):821–836.
48. Ainscow EK, Zhao C, Rutter GA. Acute overexpression of lactate dehydrogenase-A perturbs beta-cell mitochondrial metabolism and insulin secretion. *Diabetes*. 2000;49(7):1149–1155.
49. Henquin JC. The dual control of insulin secretion by glucose involves triggering and amplifying pathways in β cells. *Diabetes Res Clin Pract*. 2011;93(Suppl 1):S27–S31.
50. Martinez-Sanchez A, et al. Disallowance of Acot7 in β cells is required for normal glucose tolerance and insulin secretion. *Diabetes*. 2016;65(5):1268–1282.
51. Gleason CE, Lu D, Witters LA, Newgard CB, Birnbaum MJ. The role of AMPK and mTOR in nutrient sensing in pancreatic beta-cells. *J Biol Chem*. 2007;282(14):10341–10351.
52. Bonner-Weir S. Morphological evidence for pancreatic polarity of beta-cell within islets of Langerhans. *Diabetes*. 1988;37(5):616–621.
53. Bader E, et al. Identification of proliferative and mature β cells in the islets of Langerhans. *Nature*. 2016;535(7612):430–434.
54. Yuan T, et al. Reciprocal regulation of mTOR complexes in pancreatic islets from humans with type 2 diabetes. *Diabetologia*. 2017;60(4):668–678.
55. Del Guerra S, et al. Functional and molecular defects of pancreatic islets in human type 2 diabetes. *Diabetes*. 2005;54(3):727–735.
56. Solimena M, et al. Systems biology of the IMIDIA biobank from organ donors and pancreatectomised patients defines a novel transcriptomic signature of islets from individuals with type 2 diabetes. *Diabetologia*. 2018;61(3):641–657.
57. Cokorinos EC, et al. Activation of skeletal muscle AMPK promotes glucose disposal and glucose lowering in non-human primates and mice. *Cell Metab*. 2017;25(5):1147–1159.e10.
58. Myers RW, et al. Systemic pan-AMPK activator MK-8722 improves glucose homeostasis but induces cardiac hypertrophy. *Science*. 2017;357(6350):507–511.
59. Stancill JS, Osipovich AB, Cartailler JP, Magnuson MA. Transgene-associated human growth hormone expression in pancreatic β cells impairs identification of sex-based gene expression differences. *Am J Physiol Endocrinol Metab*.

2019;316(2):E196–E209.
60. Marchetti P, et al. The endoplasmic reticulum in pancreatic beta cells of type 2 diabetes patients. *Diabetologia*. 2007;50(12):2486–2494.
61. Galluzzi L, et al. Cell death modalities: classification and pathophysiological implications. *Cell Death Differ*. 2007;14(7):1237–1243.
62. Kroemer G, et al. Classification of cell death: recommendations of the Nomenclature Committee on Cell Death 2009. *Cell Death Differ*. 2009;16(1):3–11.
63. Weibel ER, Kistler GS, Scherle WF. Practical stereological methods for morphometric cytology. *J Cell Biol*. 1966;30(1):23–38.
64. Martin M. Cutadapt removes adapter sequences from high-throughput sequencing reads. *EMBnet J*. 2011;17(1):10–12.
65. Wu TD, Watanabe CK. GMAP: a genomic mapping and alignment program for mRNA and EST sequences. *Bioinformatics*. 2005;21(9):1859–1875.
66. Anders S, Pyl PT, Huber W. HTSeq--a Python framework to work with high-throughput sequencing data. *Bioinformatics*. 2015;31(2):166–169.
67. Love MI, Huber W, Anders S. Moderated estimation of fold change and dispersion for RNA-seq data with DESeq2. *Genome Biol*. 2014;15(12):550.